Hubble Space Telescope observations of SV Cam - I. The importance of unresolved star-spot distributions in light-curve fitting

S. V. Jeffers, J. R. Barnes, A. Collier Cameron, J.-F. Donati

Mon. Not. R. Astron. Soc. **366,** 667–674 (2006) doi:10.1111/j.1365-2966.2005.09905.x

Hubble Space Telescope observations of SV Cam – I. The importance of unresolved star-spot distributions in light-curve fitting

S. V. Jeffers,[1,2]★ J. R. Barnes,[2] A. Collier Cameron[2] and J.-F. Donati[1]

[1]*Laboratoire d'Astrophysique de Toulouse-Tarbes, Observatoire Midi-Pyrénées, 14, avenue Edouard Belin, F-31400 Toulouse, France*
[2]*School of Physics and Astronomy, University of St Andrews, North Haugh, St Andrews, Fife KY16 9SS*

Accepted 2005 November 19. Received 2005 September 2; in original form 2005 March 7

ABSTRACT

We have used maximum entropy eclipse-mapping to recover images of the visual surface brightness distribution of the primary component of the RS CVn eclipsing binary SV Cam, using high-precision photometry data obtained during three primary eclipses with Space Telescope Imaging Spectrograph aboard the *Hubble Space Telescope* (*HST*). These were augmented by contemporaneous ground-based photometry secured around the rest of the orbit. The goal of these observations was to determine the filling factor and size distribution of star-spots too small to be resolved by Doppler imaging. The information content of the final image and the fit to the data were optimized with respect to various system parameters using the χ^2 landscape method, using an eclipse-mapping code that solves for large-scale spot coverage. It is only with the unprecedented photometric precision of the *HST* data (0.000 15 mag) that it is possible to see strong discontinuities at the four contact points in the residuals of the fit to the light curve. These features can only be removed from the residual light curve by the reduction of the photospheric temperature, to synthesize high unresolvable spot coverage, and the inclusion of a polar spot. We show that this spottedness of the stellar surface can have a significant impact on the determination of the stellar binary parameters and the fit to the light curve by reducing the secondary radius from 0.794 ± 0.009 to $0.727 \pm 0.009\,\mathrm{R}_{\odot}$. This new technique can also be applied to other binary systems with high-precision spectrophotometric observations.

Key words: stars: activity – binaries: eclipsing – stars: individual: SV Cam – stars: spots.

1 INTRODUCTION

Star-spots and other forms of magnetic activity are prevalent on rapidly rotating stars with temperatures low enough to have outer convective zones. The dynamo activity in these rapidly rotating cool stars leads to the suppression of convection over large areas of the stellar photosphere. These giant star-spots can modulate the light of such active stars as they rotate by up to tens of per cent. In general, stars that exhibit this type of activity are solar-type stars with rotational periods of less than 1 d. This rapid rotation is seen in half the G and K dwarfs in open clusters younger than 100 Myr, and may also persist into middle age through tidal locking in a close binary systems such as RS CVns.

Doppler imaging is a powerful tool for determining where spots congregate on the stellar surface, but it is less successful at determining how much overall spot activity is present. Other methods such as TiO-band monitoring studies (O'Neal, Neff & Saar 1998) indicate that between 30 and 50 per cent of the stellar surface is spotted compared to 10–15 per cent from Doppler imaging (Jeffers, Barnes & Collier Cameron 2002). The discrepancy in these methods can be accounted for if the stellar surface is heavily covered by spots that are too small to be resolved through Doppler imaging. To try to resolve this we have used the photometric capabilities of the *Hubble Space Telescope* (*HST*) [signal-to-noise ratio (S/N) $\simeq$ 5000] to eclipse-map the inner face of the F9V primary of the eclipsing binary SV Cam. Using these observations, Jeffers et al. (2005) found that the surface flux in the low-latitude region to be approximately 30 per cent lower than the best-fitting PHOENIX model atmosphere. A possible cause of this flux deficit is that the surface of the primary star is peppered with unresolvable spots. They also found that when the 30 per cent spottedness is extended to the entire stellar surface there still remains a flux deficit, which could be explained by the presence of a large polar cap.

In this paper, we use the maximum entropy eclipse-mapping code DOTS (Collier Cameron 1997; Collier Cameron & Hilditch 1997) to first solve for the system parameters of the light curve, and then reconstruct the surface brightness distribution of the primary star of SV Cam. We also show how a synthetic polar cap and the star being peppered with spots below the resolution limits of eclipse-mapping are essential parameters for obtaining a good light-curve fit.

★E-mail: jeffers@ast.obs-mip.fr

Table 1. Journal of observations for SV Cam using the STIS onboard the *HST*.

Visit	Observation date	Frame no.	UT start	UT end	Julian date (+522 10)	Exposure time (s)	Phase range
1	2001 November 01	1–48	21:04:33	21:47:44	4.8793 94–4.908 758	30	0.901–0.950
		49–107	22:24:18	23:17:41	4.9093 83–4.971 851	30	0.952–1.058
		108–165	00:00:23	00:51:58	5.0015 05–5.037 328	30	1.107–1.168
2	2003 November 01	166–213	14:43:36	15:26:47	6.614 915–6.644 280	30	0.828–0.877
		214–272	16:02:23	16:55:46	6.669 628–6.706 701	30	0.920–0.983
		273–330	17:38:27	18:30:02	6.736 343–6.772 167	30	1.033–1.093
3	2005 November 01	331–378	14:43:36	15:26:47	8.416 575–8.446 561	30	0.865–0.916
		379–437	16:02:23	16:55:46	8.470 752–8.507 825	30	0.957–1.019
		438–495	17:38:27	18:30:02	8.537 468–8.573 291	30	1.069–1.13

2 OBSERVATIONS

SV Cam (F9V+K4V, P = 0.59 d, vsini = 102 km s^{-1}, $i = 90^{\circ}$) is a totally eclipsing, short-period binary system originally identified by Guthnick (1929). Contemporaneous *HST* and ground-based observations were obtained to eclipse-map SV Cam. The ground-based photometric observations were obtained to complete the light curve outside primary eclipse making it possible to determine any global asymmetry in the light curve due to the presence of any uneclipsed spots.

2.1 *HST* observations

We observed three primary eclipses of SV Cam during three *HST* visits at intervals of 2 d in 2001 between November 1 and 5. A total of nine spacecraft orbits were devoted to the observations. The G430L grating of Space Telescope Imaging Spectrograph (STIS) was used to disperse starlight over 2048 CCD elements. The observations are summarized in Table 1 and the light curve for each visit is shown in Fig. 1.

The observations cover a wavelength range from 2900 to 5700 Å, with an exposure time of 30 s and a cadence of 40 s. The exposure time was chosen as a trade-off between maximizing S/N per exposure and minimizing the time interval between observations. The total count over the entire detector is 9.4×10^7 electrons per exposure, with the photometric precision calculated to be 0.000 15 mag (S/N = 5000). The main source of systematic error, due to the subtle motion of the satellite, was removed by cross-correlating each frame with respect to a template spectrum, and then adding or subtracting a scaled number of counts. After correcting for this 'jitter' the rms scatter was consistent with the error expected from photon noise.

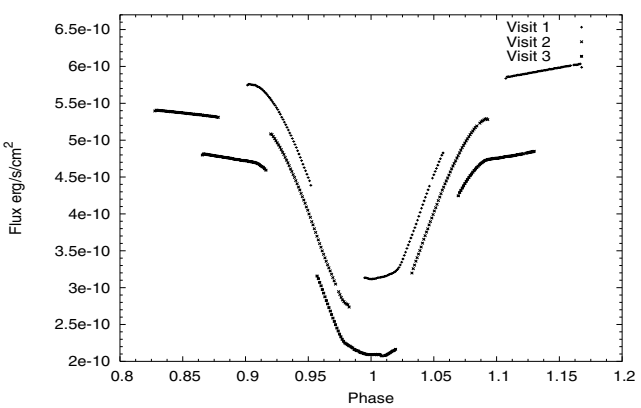

Figure 1. The comprising sections of the primary eclipse from each of the three *HST* visits, with an offset of 5×10^{-11} erg s^{-1} cm^{-2} for clarity.

2.2 Ground-based photometry

The ground-based photometric observations were obtained with the 0.93-m James Gregory Telescope (JGT) at the University of St Andrews, using a Wright Instruments CCD camera mounted at the Cassegrain focus. The observations were made with a narrow-band filter whose 85 Å(full width at half-maximum) bandpass is centred at 5300 Å, close to the *V* band. Using an exposure time of 60 s, we obtained a photometric precision of ±0.006 mag in good photometric conditions. The overhead for the chip readout between 60-s observations is typically 15 s, giving an overall sampling interval of 75 s. Observations were made over a 2-week period centred at the time of the *HST* observations. The weather permitted the observation of four full primary eclipses and three full secondary eclipses over this period.

3 DATA PROCESSING

3.1 Data reduction

Reduction of the *HST* data comprised calibrating the two-dimensional CCD images and extracting one-dimensional spectra using the standard STIS data reduction pipeline. A detailed description of this procedure is contained in the STIS handbook. This pipeline routine produces bias- and dark-subtracted, flat-fielded wavelength-calibrated images, i.e. auto-wavecal. The auto-wavecal was disabled for these images, but instead two 'guest observer' wavecals were taken per orbit. Cosmic rays were removed using an algorithm that identifies and rejects cosmic rays and other non-repeatable defects by comparing successive frames.

The ground-based photometric data were reduced using JGTPHOT, a software package developed for use with the JGT at St Andrews (Bell, Hilditch & Edwin 1993). The resulting light curves are calculated as differential magnitude values with respect to the marked comparison and check stars.

3.2 Time correction of *HST* data set

As the time of the extracted one-dimensional spectra that is output from the standard STIS data reduction pipeline (calstis) is in UT, it is necessary to apply a further time correction to this value. The heliocentric correction due to the motion of the Earth around the Sun, and due to the orbital motion of the satellite was determined through use of the 'odelaytime' routine. To convert UT into atomic time 32

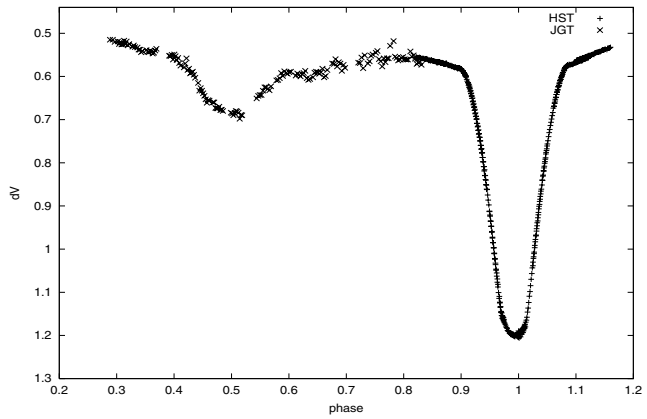

Figure 2. Interpolated *HST* data set (primary eclipse) plotted with JGT data set (secondary eclipse).

leap seconds were added, and to convert atomic time into terrestrial time 32.184 s were added, resulting in the correct terrestrial time value. Absolute precision in *HST* time is required as it is necessary to have the primary eclipse of the *HST* and of the ground-based observations exactly aligned.

3.3 Interpolation of data sets

In order to analyse the absolute spectrophotometry from STIS together with the ground-based differential photometry, it was necessary to place the magnitudes derived from the two instruments on a common magnitude scale. We constructed a synthetic filter, V_{HST}, with a bandpass and effective wavelength matching those of the filter used for the JGT observations, (bandpass of 80 Å and effective wavelength 5300 Å) and applied it to the *HST* observations. Similarly, we constructed a digital version of the Johnson B filter, B_{HST}.

At the time of each JGT flux measurement during primary eclipse we interpolated the V_{HST} magnitude and the $(B_{HST} - V_{HST})$ colour index from the two nearest points bracketing the same phase. The colour equation relating the two magnitude systems was then derived by a linear least-squares fit to the plot of $\delta V_{\rm JGT} - V_{HST}$ versus $(B_{HST} - V_{HST})$, as shown in Fig. 2. This yielded the colour equation

$$\delta V_{\rm JGT} - V_{HST} = \alpha(B_{HST} - V_{HST}) + \beta, \tag{1}$$

where the coefficient of the colour term $\alpha = -0.072\,5392 \pm 0.058\,36$ mag and the zero-point $\beta = -8.693\,67 \pm 0.033\,18$ mag.

Using this linear calibration, all of the V_{HST} magnitudes were converted to the JGT system. This procedure takes account of the zero-point offset, the effect of the V_{HST} and the JGT observations having slightly different effective wavelengths and the different spectral responses of the two filter sets and the two CCDs. The interpolated *HST* data set is shown in Fig. 2 along with the JGT data.

4 LIGHT-CURVE FITTING

The combined *HST* and JGT light curve of SV Cam is fitted using the maximum entropy code DOTS. Included in DOTS is the ability to incorporate the surface geometry and radial velocity variations of tidally distorted close binary components (Collier Cameron 1997) while solving for star-spot coverage.

4.1 Eclipse-mapping

By using eclipse-mapping, it is possible to determine the detailed locations of low-latitude spots on the stellar surface. If spots are present on the inner surface of the primary, that is occulted by the cooler secondary star, jagged discontinuities will be produced on the eclipse profile as the primary is occulted by the secondary. The time-scales and amplitudes of these discontinuities will reflect the distribution of spot sizes on the inner surface of the primary.

4.1.1 Maximum entropy

The maximum entropy method allows us to determine the simplest image of the surface of the primary star (in terms of its information content as quantified by the Shannon–Jaynes image entropy), that can reproduce, at a specified goodness of fit, the perturbations to the primary eclipse.

For images where the mapping parameter f_i is bolometric surface brightness and so can take any positive value, the entropy takes the form

$$S = \sum_i \left[f_i - m_i - f_i \ln\left(\frac{f_i}{m_i}\right)\right]. \tag{2}$$

Here, m_i is the default value that a pixel will have when there are no other constraints imposed by the data. In this analysis a restricted form of the entropy is used as the filling-factor model has been adopted. This combines the entropy of the spot image f_i and of the photospheric image $(1 - f_i)$:

$$S = \sum_i \left[-f_i \ln\left(\frac{f_i}{m_i}\right) - (1 - fi)\ln\left(\frac{1 - f_i}{1 - m_i}\right)\right]. \tag{3}$$

To construct the final image, the values for the spot and photospheric f_i are iteratively adjusted to maximize;

$$Q = S - \lambda\chi^2. \tag{4}$$

This is equivalent to maximizing the entropy S over the surface of a hyper-ellipsoid, of constant χ^2, in image space. This is bounded by the constraint surface at some fixed value of χ^2. The Lagrange multiplier, λ, is set so that the final solution lies on a surface with $\chi^2 \simeq M, M$ being the number of measurements in the data set. By setting a Lagrangian multiplier, it is possible to determine the extremum (maximum) of the entropy, the image with the least information content, subject to the constraint of obtaining the best fit to the data. A more detailed explanation of this, and other methods, is discussed by Collier Cameron (2001).

It is important not to overfit χ^2 during the reconstruction, as this can result in an ill photometric fit and artefacts on the final spot map. The number of iterations was set to 25, as through rigorous testing we found this to be the value where the final image did not contain any distortions due to ill fitting.

4.2 Geometric parameters

The success of a surface image reconstruction depends largely on a correct determination of the geometric parameters of the binary system (Vincent et al. 1993). Independent reconstructions for the star-spot parameters and the geometric parameters of the system, are susceptible to the distortions in the light curve yielding the wrong system parameters or vice versa. If the system parameters are wrong, in general a satisfactory fit to the data is only obtained by increasing the amount of structure in the stellar surface brightness distribution,

Table 2. Summary of observed stellar parameters for SV Cam from the literature where $T_{\rm pri}$ and $T_{\rm sec}$ are the primary and secondary photospheric temperatures (K), $R_{\rm pri}$ and $R_{\rm sec}$ are the primary and secondary radii (in units of $R_\odot$), i is the binary system inclination (degrees), q is the secondary to primary mass ratio and S/P indicates spectroscopic or photometric observations.

Reference	$T_{\rm pri}$	$T_{\rm sec}$	$R_{\rm pri}$	$R_{\rm sec}$	i	q	S / P	Spectral type
This work	6038(58)	4804(143)	1.238(6)	0.794(6)			P	F9V+K4V
(reduced $T_{\rm phot}$ plus polar cap)	5935(38)	4808(143)	1.235(7)	0.727(6)			P	G0V+K4V
Lehmann, Hempelmann & Wolter (2002)			1.18(2)	0.76(2)	90.0	0.642(5)	S	G0V+K6V
Rucinski et al. (2002)					90.0	0.641(7)	S	G2V (primary plus secondary)
Kjurkchieva, Marchev & Zola (2002)			1.38(5)	0.94(6)	80.0	0.593(11)	S	F5V+G8V
Albayrak et al. (2001)	6440	4467(34)	1.38(2)	0.87(2)	89.6(9)	0.56	P	F8V+K6V
Albayrak et al. (2001)	6200	4377(32)	1.38(2)	0.87(2)	89.6(9)	0.56(10)	P	F5V+K6V
Pojmanski (1998)			1.25	0.8	90.0	0.56(9)	S	F5V+K0V
Patkos & Hempelmann (1994)	5750	4500	1.18(5)	0.75(3)			P	G2/3V+K4/5
Rainger, Hilditch & Edwin (1991)					90.0	0.7	S	G2/3V+K4V
Zeilik et al. (1988)	5800	4300	1.17(3)	0.74(3)	89.5(5)		P	G3V
Budding & Zeilik (1987)	5750	4500	1.11(2)	0.74(2)	90.0(5)	0.71	P	G3V+K4
Hilditch, McLean & Harland (1979)	5800	4140	1.224	0.864	80.0	0.7	P	G3V+K4V

usually leading to a greater total spot area than is present when the correct geometric parameters are used.

The principal parameters that affect the shape of the light curve of an unspotted star are the relative temperatures, the radii of the two stars and the system inclination. The relative surface brightnesses of the two components determine the relative depths of the primary and secondary eclipses. The radii of the two stars and the binary system inclination are related to each other by the orbital phases at which the four contact points occur (phases 0.906, 0.977, 1.023 and 1.093, respectively). These relations are further complicated by the presence of star-spots which in general have the effect of altering the depth of the eclipses and making the contact points asymmetrical.

SV Cam has been the subject of numerous photometric and spectroscopic studies. Despite this, there still does not exist an established and reliable set of stellar parameters. The various published combinations of stellar parameters that can be found for SV Cam in the literature are summarized in Table 2. A discussion of the individual merits of each set of binary system parameters is beyond the scope of this paper. Given the wide range of geometric parameters available for SV Cam, it was necessary to determine a set of parameters that would give an optimal fit to our light curve.

In fitting the photometric light curve of SV Cam we use the mass ratio ($q = 0.641 \pm 0.007$), semi-amplitude velocity ($K_1 = 121.86 \pm 0.76$, $K_2 = 190.17 \pm 1.73$) and systematic radial velocity (-9.31 ± 0.78) of Rucinski et al. (2002), as their solution for spectroscopic orbit of SV Cam is very well defined.

4.3 Temperature

Jeffers et al. (2005) determined the temperature of the separated primary and secondary components of SV Cam using PHOENIX (Allard, Hauschildt & Schweitzer 2000) model atmosphere spectra. Model atmospheres, ranging in temperature from 5600 to 6500 K in 100-K steps, were fitted to the spectrum of the primary and secondary stars using χ^2 minimization. The minimum χ^2 value corresponds to a temperature of 6013 ± 19 and 4804 ± 143 K for the primary and secondary stars, respectively. The primary star was then isolated and fitted using the same method, where the minimum temperature is 6038 ± 58 K. In this work we use the independently fitted primary temperature, as the error estimate is more reliable.

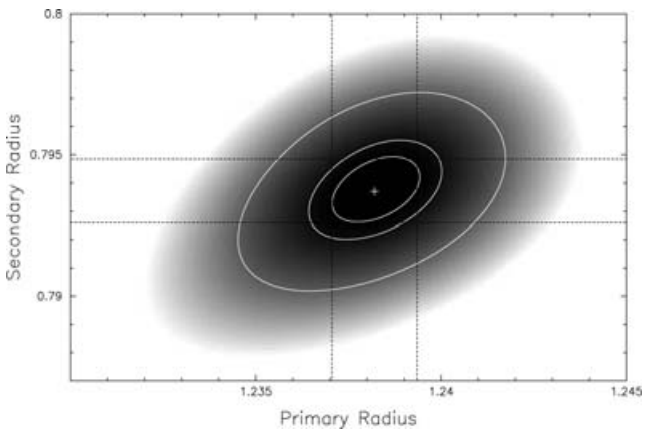

Figure 3. Contour plot of the χ^2 landscape for the primary and secondary radii. From the centre of the plot, the first contour ellipse is the one-parameter 1σ confidence limit at 63.8 per cent, the second contour ellipse is the two-parameter 1σ confidence limit at 63.8 per cent, and the third contour ellipse is the two-parameter 2.6σ confidence limit at 99 per cent.

4.4 Radii

The radii for the primary and secondary stars were determined using the robust grid search method. This method uses a grid of radii as input to DOTS ranging from 1.17 to 1.26 $R_\odot$ for the primary star and 0.73 to 0.82 $R_\odot$ for the secondary star in 0.005-$R_\odot$, intervals. For each grid point, a model with the specified set of geometric parameters was iterated 25 times to obtain the lowest value of the reduced χ^2. The inclination was not included as it scales as $(\sin i)^{-1}$, implying a negligible difference between inclinations of 90° and 85°.

The results for the χ^2 minimization are shown in Fig. 3 in the form of a contour plot. The minimum χ^2 value occurs at 1.238 ± 0.007 and 0.794 ± 0.009 $R_\odot$ for the primary and secondary stars, respectively. The best-fitting stellar parameters for the combined JGT and *HST* data sets are summarized in Table 3.

4.5 Light-curve fit and surface brightness image

The resulting maximum entropy fit to the light curve, using the stellar parameters as previously defined is shown in Fig. 4. The observed data minus computed residual light curves are shown in

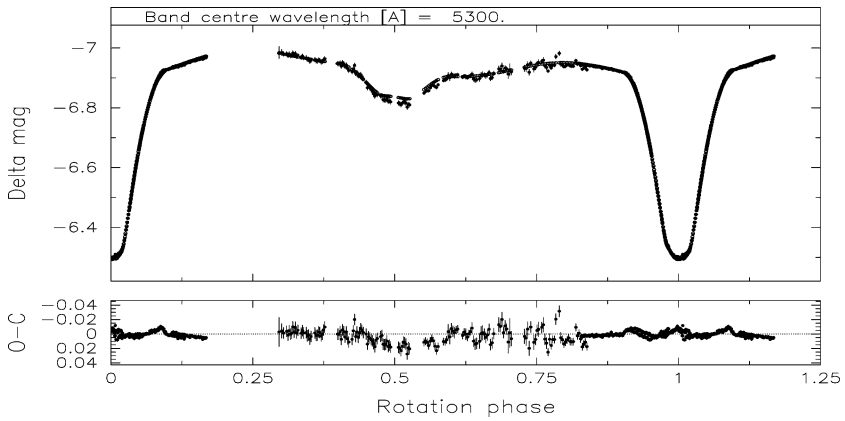

Figure 4. Combined *HST* and JGT light curves, with a maximum entropy fit.

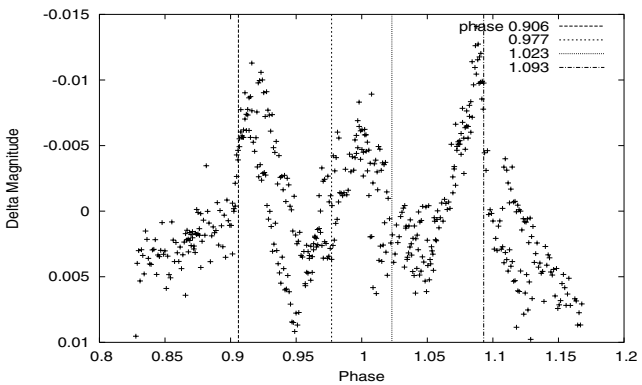

Figure 5. Observed minus computed residuals with no polar cap (*HST* data only). The four contact points are shown as vertical lines.

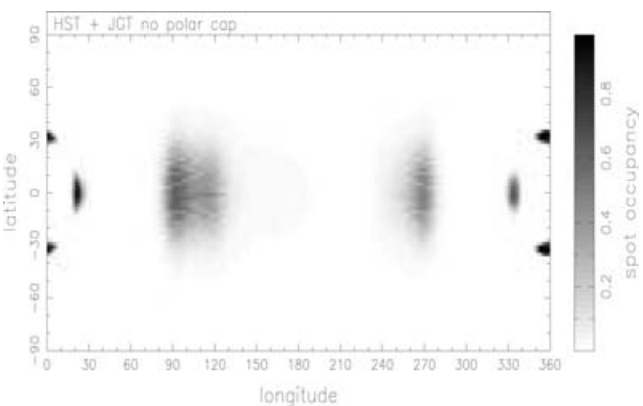

Figure 6. The final spot map of SV Cam (*HST* plus JGT data). Note that phase runs in reverse to longitude. Spots reconstructed using χ^2 and located at the quadrature points have been shown by Jeffers (2005) to be spurious. Note that phase runs in reverse to longitude.

Fig. 5 in enlarged form covering just the *HST* primary eclipse data. The stellar surface image that results from these fits is shown in Fig. 6.

The model light curve of the best-fitting binary system parameters is shown in Fig. 4. When the modelled light curve is subtracted from the observed data the residuals are symmetric about phase 1, and have two large discontinuities that occur at the first and fourth contact points either side of the primary eclipse (Fig. 5). Given the location of these discontinuities, an obvious explanation would be that the radius of either of the two stars has been incorrectly determined. However, the accuracy of our determination of the stellar parameters, as described in Section 4, can eliminate this possibility.

The surface brightness distribution (Fig. 6) shows two Large-spot features at the quadrature points similar to 'active longitudes' that have been observed using photometry on other RS CVns (e.g. Olah, Hall & Henry 1991; Lanza et al. 2001, 2002). These spots are reconstructed at the equator as there is no eclipse information to determine the latitude. The spot at 100° is stronger as that quadrature of the star has a higher spot coverage, which is also evident in the lower light level of the photometric light curve at phase ≈0.75. The spots reconstructed at 25°, 335° and 360° result from spots on the primary star that have been occulted by the secondary star during primary eclipse. The symmetry is due to the inability of DOTS to determine the hemisphere of the spot feature.

5 UNRESOLVABLE SPOT COVERAGE

5.1 Reduced photospheric temperature

Jeffers (2005) tested the limitations of surface brightness images from photometric data by modelling many subresolution spots on an immaculate SV Cam. Surface brightness distributions reconstructed from these synthetic light curves show distinctive spots at the quadrature points. The presence of similar spot features in Fig. 6 could indicate that the surface of SV Cam is peppered with many spots that are below the resolution capabilities of the eclipse-mapping technique. This would then be consistent with the results of TiO-band monitoring studies (O'Neal et al. 1998) which show that between 30 and 50 per cent of the surface of a star may be spotted.

Further evidence for the peppering of the primary star of SV Cam by small star-spots is shown by Jeffers et al. (2005). As previously described in Section 4, they determined the temperatures of the two stars using best-fitting PHOENIX model atmospheres. It was also found that the surface flux of the primary star is approximately 28 per cent lower than that predicted by a PHOENIX model atmosphere at the best-fitting effective temperature. Even taking into account the spot distributions as shown in Fig. 6, this flux deficit can only be accounted for if the surface of the primary star is peppered with unresolved spots. As these spots are not resolvable using the eclipse-mapping technique, they can lead to an

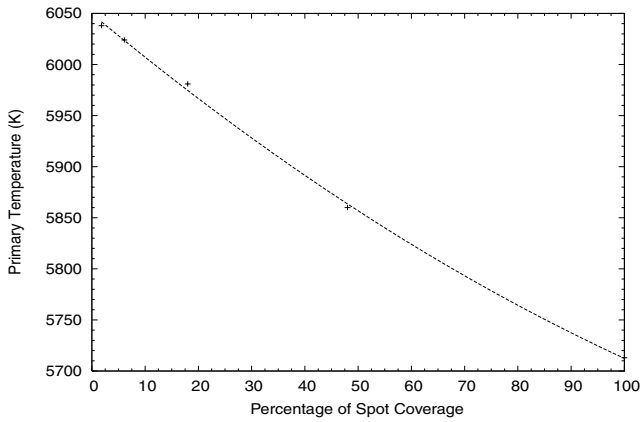

Figure 7. The decrease of photospheric temperature of the primary star as a function of percentage of spot coverage on its surface.

underestimation of the photospheric temperature of the star and will have the effect of decreasing the flux deficit during the eclipse at all wavelengths.

To determine the reduced photospheric temperature, resulting from the presence of many unresolvable spots, we extend the work of Jeffers (2005). An extrapolated solar spot size distribution is applied to an immaculate SV Cam, for 1.8, 6.1, 18, 48 and 100 per cent area filling factors of spots, with $T_{\rm ph} = 6038$ K and $T_{\rm sp} = 4538$ K. Each of these spot distributions is modelled as a photometric light curve, and is then used as input to the maximum entropy eclipse-mapping code. To obtain a satisfactory fit to the light curve it was necessary to reduce the photospheric temperature to values as shown in Fig. 7. A quadratic fit to these points gives a temperature for 28 per cent spottedness of 5935 K which is the average temperature over hotter and unresolvable cooler temperature regions.

5.2 Polar spot

The work of Jeffers et al. (2005) also showed that in addition to the 28 per cent spot coverage in the eclipsed region of the primary star, there is an additional 12.5 per cent flux deficit in non-eclipsed regions of the star. The additional flux deficit can only be explained by the presence of a polar cap which would have the effect of increasing the depth of the primary eclipse, and would lead to an incorrect light-curve solution.

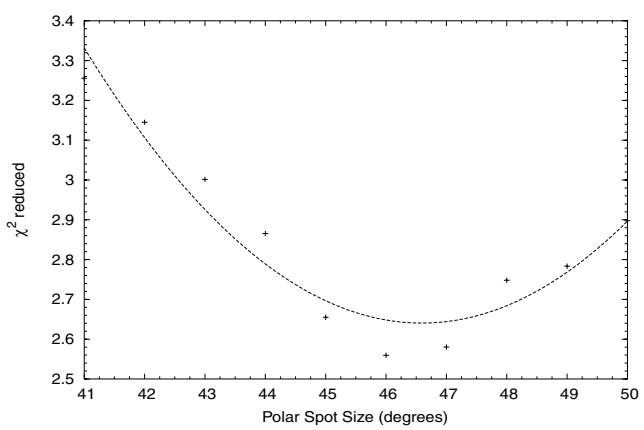

Figure 8. Quadratic fit to the variation of χ^2 as a function of polar spot size.

Table 3. Geometric binary system parameters computed for SV Cam. For solution 1, the primary and secondary temperatures are taken from Jeffers et al. (2005), while solution 2 shows the radii and polar cap size solved using a reduced photospheric temperature to synthesize the star being peppered with small spots.

Parameter	Solution 1	Solution 2
Ephemeris	52214.34475 (MJD)	
$T_{\rm pri}$	6038 ± 58 K	5935 ± 38 K
$T_{\rm sec}$	4804 ± 143 K	4804 ± 143 K
$R_{\rm pri}$	$1.238 \pm 0.006\,{\rm R}_\odot$	$1.235 \pm 0.007\,{\rm R}_\odot$
$R_{\rm sec}$	$0.794 \pm 0.006\,{\rm R}_\odot$	$0.727 \pm 0.006\,{\rm R}_\odot$
Polar cap		46.7°

We include a polar cap in our light-curve solution by extending the two-dimensional grid search described in Section 4 to a three-dimensional grid search including the polar spot size from 35° to 50°. The polar spot is assumed to be at 4500 K, circular, centred at the pole, and is in addition to the reduced photospheric temperature as described above. For each polar spot size, the minimum primary and secondary radii are determined using a χ^2 contour map. These minimum χ^2 values are plotted as a function of polar spot size in Fig. 8. The best-fitting polar cap size, 46.7° was determined from the minimum of a quadratic function fitted to these points. This value is in good agreement with the independently determined value of $42 \pm 6°$ by Jeffers et al. (2005). The grid search of radii is then repeated using a fixed value for the polar spot size. The results for the χ^2 minimization are summarized in Table 3 and are shown as a contour map in Fig. 9.

5.3 Final light-curve fit

The best-fitting stellar parameters are used to create a maximum entropy light-curve fit (Fig. 10) and stellar surface brightness image for the primary star (Fig. 11). The observed data minus computed residual light curve for the primary eclipse, as shown in Fig. 12, is significantly flatter than the residuals shown in Fig. 5. The secondary eclipse shows also a better fit than that in Fig. 4. The reduced

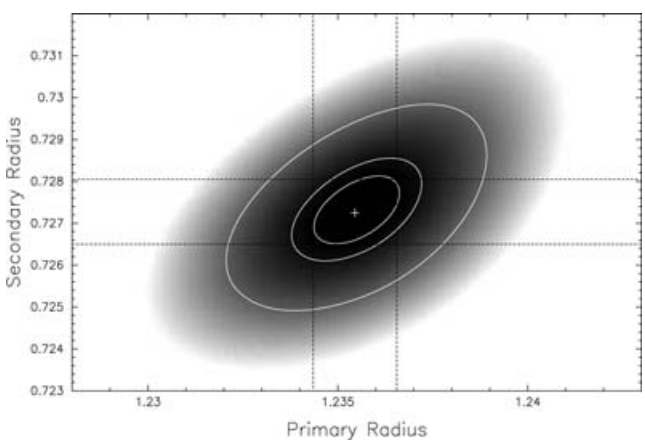

Figure 9. Contour plot of the χ^2 landscape for the primary and secondary radii with a 46.69° polar spot. From the centre of the plot, the first contour ellipse is the one-parameter 1σ confidence limit at 63.8 per cent, the second contour ellipse is the two-parameter 1σ confidence limit at 63.8 per cent, and the third contour ellipse is the two-parameter 2.6σ confidence limit at 99 per cent.

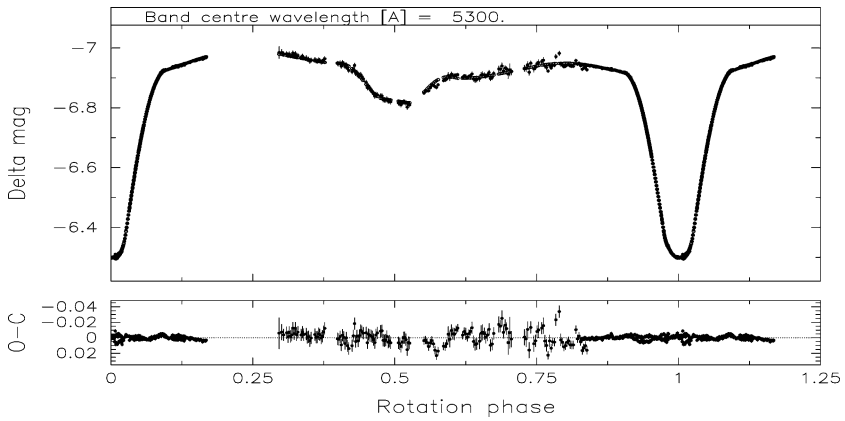

Figure 10. Combined *HST* and JGT light curves, with a maximum entropy fit with a polar cap and reduced photospheric temperature included.

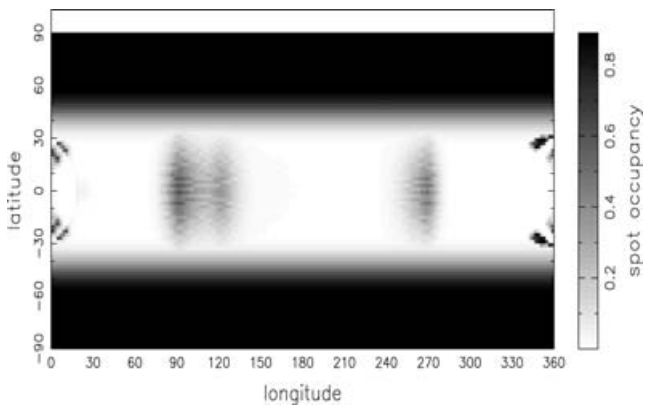

Figure 11. The final spot map of SV Cam (*HST* plus JGT data) with two 46.7° polar caps and reduced photospheric temperature. Note that phase runs in reverse to longitude. Spots reconstructed using χ^2 and located at the quadrature points have been shown by Jeffers (2005) to be spurious as they can be reconstructed from models of high star-spot coverage. Note that phase runs in reverse to longitude.

χ^2 value after 25 iterations was 2.05, which is slightly reduced from the value of 3.55 obtained without a polar spot and a reduced photospheric temperature. This result shows that the presence of a polar cap and subresolution spots have a significant influence on the O–C residuals.

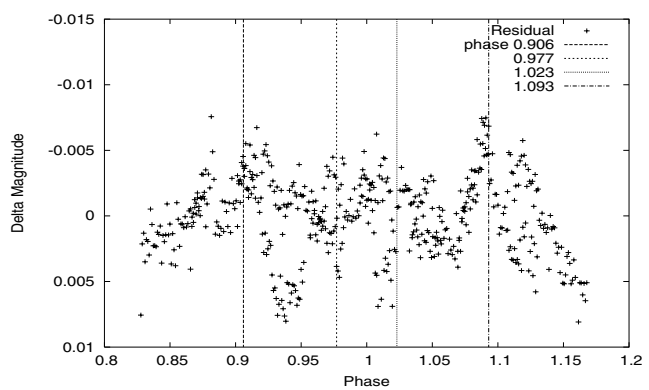

Figure 12. Observed minus computed residuals for the case with a reduced photospheric temperature and a polar cap of 46.69° radius. The four contact points are shown as vertical lines.

The maximum entropy surface brightness distribution, as shown in Fig. 11, is similar to that shown in Fig. 6. The spot feature at 0° and 360° is not an artefact as it is in the eclipse path of the secondary, but results from time-variable structure in the base of the primary eclipse. It is a symmetric spot feature as image reconstructions from photometry are not able to determine the latitude of a spot. The spot feature at 25° and 335° in Fig. 6 has disappeared due to the correct determination of the temperature of the primary star and consequently the radius of the secondary star.

6 DISCUSSION AND CONCLUSIONS

We have used eclipse-mapping, based on the maximum entropy method to recover images of the visual surface brightness distribution of the primary component of the RS CVn eclipsing binary SV Cam. It is only with the unprecedented photometric precision of the *HST* data that it is possible to see strong discontinuities at the four contact points in the residuals of the fit to the light curve. These features can only be removed from the O–C light curve by the reduction of the photospheric temperature, to synthesize high unresolvable spot coverage, and the inclusion of a polar spot.

In fitting the light curve of SV Cam we used the independently determined primary and secondary temperatures, as determined by Jeffers et al. (2005), as input to our solution. The primary and secondary radii were then determined using a 'grid search' method. Although the 'grid search' method is computationally intensive, it does provide reliable results. In contrast to this is the 'downhill simplex' amoeba method (Press et al. 1992) which repeatedly returned light-curve solutions from local χ^2 minima rather than from the global χ^2 minimum. The resulting parameters ($R_{\rm pri} = 1.238\,{\rm R}_\odot$ and $R_{\rm sec} = 0.794\,{\rm R}_\odot$) are in closest agreement with the values of Pojmanski (1998) derived from spectroscopic data ($R_{\rm pri} = 1.25\,{\rm R}_\odot$ and $R_{\rm sec} = 0.8\,{\rm R}_\odot$). The errors derived in this work are an order of magnitude smaller than previous light-curve solutions.

The maximum entropy fit to the data using the best-fitting orbital parameters shows strong discontinuities at the four contact points of the primary eclipse. When we reconstructed an image using *only* the ground-based JGT data (photometric precision = 0.006) we found that these strong discontinuities were not visible in the residual light curve. It is only with the high photometric precision of the *HST* (0.000 15 mag or S/N 5000) that it is possible to distinguish the strong discontinuities in the residual light curve.

The surface brightness distribution shows spots at the quadrature points consistent with surface images of other RS CVns

reconstructed using χ^2 minimization, e.g. Olah et al. (1991) and Lanza et al. (2001, 2002). However, the reliability of these images has been investigated by Jeffers (2005) where spurious spots at the quadrature points have been reconstructed from a synthetic star containing a high degree of subresolution spots. This is consistent with results from other methods such as TiO-band monitoring (O'Neal et al. 1998) which indicate that between 30 and 50 per cent of the surface of a star could be covered in star-spots at all times.

A high total spot coverage on the primary star of SV Cam will modify the apparent photospheric temperature. In a related paper, Jeffers et al. (2005) showed that when the surface flux in the low-latitude eclipsed region was approximately 30 per cent lower than the best-fitting PHOENIX model atmosphere. In this paper, we showed that this is equivalent to a reduction in the photospheric temperature from 6039 ± 58 to 5935 ± 38 K. High spot coverage also has important structural implications. As investigated by Spruit & Weiss (1986), a star with high spot coverage will, over thermal time-scales, readjust its structure to compensate in radius and temperature. For example, the radius of the primary star is 10 per cent larger than that expected for its spectral type, and could provide an explanation as to the large variation in binary system parameters as shown in Table 2.

The addition of a polar spot and the reduction of the photospheric temperature has a negligible influence on the empirically determined radius of the primary star, but a more significant influence on the secondary, decreasing it from 0.794 ± 0.007 to $0.727 \pm 0.009\,\mathrm{R}_\odot$. The presence of a polar spot will increase the depth of the primary eclipse, while a reduction in the photospheric temperature will decrease the depth. In both cases, the binary system compensates for this by making the secondary star smaller as it consequently needs to eclipse less light. The standard luminosity–radius–temperature relation ($L = 4\pi R^2 \sigma T^4$) shows that if $T_{\rm pri}$ and $T_{\rm sec}$ are fixed, then the only variable parameters are the radii of the primary and secondary stars. The timing of the first and fourth contact points fixes the primary radius, leaving the secondary radius as the only adjustable parameter.

The resulting residuals from the maximum entropy light-curve fit are significantly flatter with the light-curve solution that includes a polar cap and a reduced photospheric temperature. However, there are still variations in the residual light curve, which could result from the eclipse-mapping routine interpreting small-scale variations in the light curve (i.e. unfitted spots) as noise. A 0.005-mag change as shown in Fig. 12 would result in additional 14 per cent of the area of the annulus around the secondary being spotted than is shown in the surface brightness images. However, the remaining structure in the O–C residual could result from an incorrect value of the limb darkening or the presence of plage on the surface of the primary star, which will require further investigation.

The surface brightness image reconstructed with the refined binary system parameters (Fig. 11) has reduced surface structure compared to the image reconstructed with the original parameters. This is noticeable at longitudes 25° and 335°, where the small spots have disappeared with the refined binary system parameters. The structure at longitudes 0° and 360° are not artefacts of the eclipse-mapping technique as they are in the eclipse path of the secondary, but result from time-variable structure on the surface of the primary star during primary eclipse. The features are symmetric as it is not possible to resolve the latitude of a star-spot using photometric observations. Doppler images of active stars show that polar caps do not have a uniform structure, unlike the polar caps used in our model and shown in Fig. 11.

The upcoming COROT and KEPLER missions, which are designed to detect transits eclipses of stars by terrestrial sized planets, will discover thousands of eclipsing binary stars with μmag photometry, while missions such as GAIA should deliver 10^6 new eclipsing binary stars. The benefit of such a wealth of high-precision data will be lost if it is not possible to accurately solve the binary system parameters from the light curves.

ACKNOWLEDGMENTS

We would like to thank Keith Horne for the use of his XCAL program and Roger Stapleton and Tim Lister for their guidance on the time corrections. We would like to also thank Phil Hodge at STSCI for amending the *HST* data reduction pipeline routine 'odelaytime', to account for heliocentric and satellite–Earth time corrections. SVJ acknowledges support from a PPARC research studentship and a scholarship from the University of St Andrews while at St Andrews University. SVJ also acknowledges support at OMP from a personal Marie Curie Intra-European Fellowship within the Sixth European Community Framework Programme.

REFERENCES

Albayrak B., Demircan O., Djurašević G., Erkapić S., Ak H., 2001, A&A, 376, 158
Allard F., Hauschildt P. H., Schweitzer A., 2000, ApJ, 539, 366
Bell S., Hilditch R., Edwin R., 1993, MNRAS, 260, 478
Budding E., Zeilik M., 1987, ApJ, 319, 827
Collier Cameron A., 1997, MNRAS, 287, 556
Collier Cameron A., Hilditch R. W., 1997, MNRAS, 287, 567
Guthnick P., 1929, Astron. Nachr., 235, 83
Hilditch R. W., McLean B. J., Harland D. M., 1979, MNRAS, 187, 797
Jeffers S. V., 2005, MNRAS, 359, 729
Jeffers S. V., Barnes J. R., Collier Cameron A., 2002, MNRAS, 331, 666
Jeffers S. V., Cameron A. C., Barnes J. R., Aufdenberg J. P., Hussain G. A. J., 2005, ApJ, 621, 425
Kjurkchieva D. P., Marchev D. V., Zola S., 2002, A&A, 386, 548
Lanza A. F., Catalano S., Rodonò M., İbanoğlu C., Evren S., Taş G., Çakırlı Ö., Devlen A., 2002, A&A, 386, 583
Lanza A. F., Rodonò M., Mazzola L., Messina S., 2001, A&A, 376, 1011
Lehmann H., Hempelmann A., Wolter U., 2002, A&A, 392, 963
Olah K., Hall D. S., Henry G. W., 1991, A&A, 251, 531
O'Neal D., Neff J., Saar S., 1998, ApJ, 507, 919
Patkos L., Hempelmann A., 1994, A&A, 292, 119
Pojmanski G., 1998, Acta Astron., 48, 711
Press W. H., Teukolsky S. A., Vetterling W. T., Flannery B. P., 1992, Numerical Recipes in FORTRAN. The Art of Scientific Computing, 2nd edn. Cambridge Univ. Press, Cambridge
Rainger P. P., Hilditch R. W., Edwin R. P., 1991, MNRAS, 248, 168
Rucinski S. M., Lu W., Capobianco C. C., Mochnacki S. W., Blake R. M., Thomson J. R., Ogloza W., Stachowski G., 2002, AJ, 124, 1738
Spruit H. C., Weiss A., 1986, A&A, 166, 167
Vincent A., Piskunov N. E., Tuominen I., 1993, A&A, 278, 523
Zeilik M., de Blasi C., Rhodes M., Budding E., 1988, ApJ, 332, 293

This paper has been typeset from a TEX/LATEX file prepared by the author.